Rijksuniversiteit Groningen

Bachelor Thesis

A Phenomenological Model for Early Galaxy Evolution

Author:
J.G.E. Straat

Supervisor:
Prof Dr P. Dayal

Abstract

This thesis aims to put constraints on the star formation efficiency and ratio between baryonic matter and dark matter, f and ρ_b/ρ_{dm} respectively, during the Epoch of Reionization. This is interesting to study as no constraints have been put on these parameters yet. In this analysis the constraints were studied for redshifts between 5 and 10. This was done by using halo mass simulations by Murray et al. (2013) and converting those into luminosity functions. For the simulations and the conversion in this thesis, the ΛCDM csmolgy was assumed. In this conversion f and ρ_b/ρ_{dm} were fitted to data by Harikane et al. (2022), Bouwens et al. (2021), Finkelstein et al. (2015), Bowler et al. (2015), Ishigaki et al. (2018), Bowler et al. (2020), Bouwens et al. (2020) and Oesch et al. (2018).

The final constraints are bounded by hyperbolas for which the limits are given in table 4.1. A phenomenological model for early galaxy evolution might be a viable explanation for the dip at the low luminosity end of the UV LF. However, a halo mass dependence on f and ρ_b/ρ_{dm} might be interesting to look at in future work.

Contents

Chapter 1

Introduction

Dark matter is the dominant source of matter in the Universe (Ryden, 2017). However, the discovery of dark matter is quite recent. The first hints at the existence of dark matter appeared at the start of the 20th century (Zwicky, 1933). When astronomers looked at the velocity distribution of galaxies, they noticed that the rotation curve was flattening in the outer parts of a galaxy. This would only be possible if there was more mass in the galaxy than the observations predicted. This missing mass has been dubbed dark matter. Dark matter would gravitationally collapse in the early Universe due to density perturbations. These density perturbations grew out to be halos. All galaxies are hosted by these dark matter halo (Wechsler & Tinker, 2018). It is therefore very important to understand the formation and evolution of these halos to better understand galaxy formation. Figure 1.1 visualizes this configuration of a galaxy and its host dark matter halo.

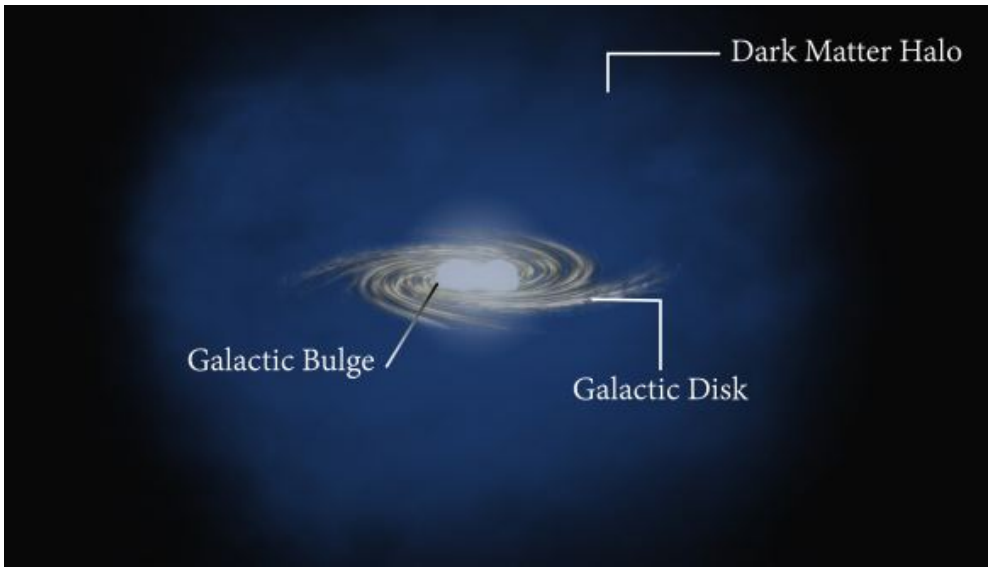

Figure 1.1: This image shows the configuration of a galaxy and its host dark matter halo. Credit: L Jaramillo and O Macias, Virginia Tech.

One of our most helpful tools in understanding the evolution of these halos, and the galaxies that they host, is the luminosity function. This function tells you the number density of halos that have a luminosity which falls within a luminosity interval. The luminosity function (LF) can have a different shape depending on what model for dark matter you are using. In this thesis, I

will use the Cold Dark Matter (CDM) model which will be further explained in section 1.1.

Unfortunately, this model does not line up with observations. The LF in CDM predicts more low luminosity halos than what we observe. This can be explained by adopting a different model for dark matter, such as Warm Dark Matter, or looking into possible processes which restrain the formation of stars.

In this thesis, I will be looking into the viability of this second explanation. To do this, I will be using simulations for the halo mass function, which gives the number density of halos that have a halo mass in a halo mass interval. These simulations will then be converted into the luminosity function again.

To perform this conversion, two parameters have to be fitted, f and ρ_b/ρ_{dm}. These are the star formation efficiency and the density ratio between baryonic matter and dark matter respectively. The ultimate goal is to put constraints on these two parameters and see if they can explain the decline at the faint end of the halo mass function. This has not been done before and could help in deciding whether this explanation is valid or that the decline could have another cause.

In the following sections, I will lay down the basic framework of this thesis, where I discuss the ΛCDM model, the Epoch of Reionization and current techniques for detecting high-redshift galaxies. In section 2, the theory behind the calculations and simulations will be explained. Followed by section 3, where the final results will be obtained, namely the constraints on f and ρ_b/ρ_{dm}. +

1.1 The ΛCDM Model

The ΛCDM model is a mathematical model that describes the current features and the evolution of the Universe and is nowadays the most widely accepted (Bullock & Boylan-Kolchin, 2017; Koppelman, 2020). According to this model, the main contributors to the energy in the Universe are dark energy, which is represented by the Λ in ΛCDM, and dark matter (Ryden, 2017). The dark matter in this model is nonrelativistic dark matter. This means that the dark matter particles have negligible to no velocity, it is therefore also dubbed cold dark matter(CDM), because it has little to no thermal velocity. Due to their dominance at $z < 0.5$, the evolution of the Universe is mainly influenced by them.

The ΛCDM model predicts the composition of the Universe in the Hot Big Bang model. In the Hot Big Bang model, the Universe was in the beginning very dense and hot. After approximately 10^{-43} seconds, this hot, dense Universe started a period called inflation (Ryden, 2017). Inflation is a period in the early Universe, where it was expanding exponentially (Ryden, 2017). This rapid expansion allowed for the formation of early density perturbations, necessary for the structures that we observe today.

One of the main outcomes of inflation is the smoothing of the Universe. This entails that after inflation the Universe was very homogeneous and isotropic, meaning that the Universe is more or less the same in every direction, and the baryonic and dark matter are well mixed. Even though the Universe was very smooth at this point, there were tiny density perturbations throughout. Hence there were parts of the Universe which were slightly under-dense and over-dense, where the over-dense regions had a density higher than the critical density and the under-dense regions had a density lower than the critical density.

If a region's density exceeds the critical density, it can gravitationally collapse. The accretion of dark matter and baryonic matter continued until potential wells were formed. If a particle has enough energy, it can escape these potential wells and the density perturbation will be flattened. The bigger the potential well, the more energy is needed to escape it. CDM has the property that it is cold, as the name might imply. This means that it has no energy itself and is thus not capable of escaping these potential wells. Therefore, potential wells at all scales can be formed without being smoothed out (Libeskind et al., 2013).

These potential wells formed the halos which host galaxies in the current Universe. Of course, bigger halos would attract other halos as well. These halos would then merge to form bigger halos. This is called hierarchical structure formation and allowed for the formation of the galaxies that we see today (Dayal et al., 2014). As mentioned previously, the baryonic and dark matter were well mixed. Hence there was plenty of baryonic matter in these halos. This matter is what eventually formed the stars and dust in galaxies.

The fraction of baryonic matter in these halos is predicted by the ΛCDM model. The model describes the density of the Universe and is often described by the density parameter,

$$\Omega_0 = \Omega_{dm} + \Omega_b + \Omega_0 + \Omega_\Lambda$$

the baryonic matter density, Ω_b, is 0.048 and the dark matter density, Ω_{dm}, is 0.262. Hence all the matter accounts for 0.31 of the energy in the Universe. The rest of the energy resides mainly in dark energy represented by the cosmological constant, $\Lambda(\Omega_\Lambda \approx 0.69)$ (Aghanim et al., 2020).

The ratio of baryonic matter and dark matter that is to be expected in these halos would be $\frac{\Omega_b}{\Omega_{dm}}$ since these two variations of matter were well mixed in the early Universe. Hence the cosmic abundances would be represented by the abundances in the halos themselves. This is a very basic model and some processes could influence this ratio. Section 2.3 will elaborate more on processes quenching the star formation and altering the ratio between baryonic matter and dark matter within the halo.

1.2 Epoch of Reionization

The Universe has undergone multiple phases in its evolution. The earliest stages were the epoch of recombination, photon decoupling and last scattering. During these epochs, the baryonic matter went from being ionized to being neutral by combining with electrons, photons scatter less from electrons and cosmic microwave background(CMB) photons interacted with an electron for the last time, respectively (Dayal & Ferrara, 2018). When these stages were finished, the Universe was about 370.000 years old and photons could decouple from neutral atoms. This is represented in Figure 1.2 by the white region in the beginning (Tanabashi et al., 2018). After this happened the CMB was created and the Universe was transparent at wavelengths longer than Lyman α (Maoz, 2016).

The stage that followed is referred to as the Dark Ages. They are called this way since no stars were formed yet and no other sources for light were around at the time. The Universe was mostly filled with neutral gas that was slowly coming together for the first stars. At this point, there were no metals in the Universe hence the cooling of the gas was very inefficient. Therefore, the first stars were big and produced large amounts of UV light. The surrounding matter was mostly neutral hydrogen, which is very optically thick for these short-wavelength photons. This made the Universe opaque to UV photons. These photons were absorbed by

the neutral hydrogen, ionizing or exciting them. This period where the neutral hydrogen got reionized, is called the Epoch of Reionization (Zaroubi, 2013).

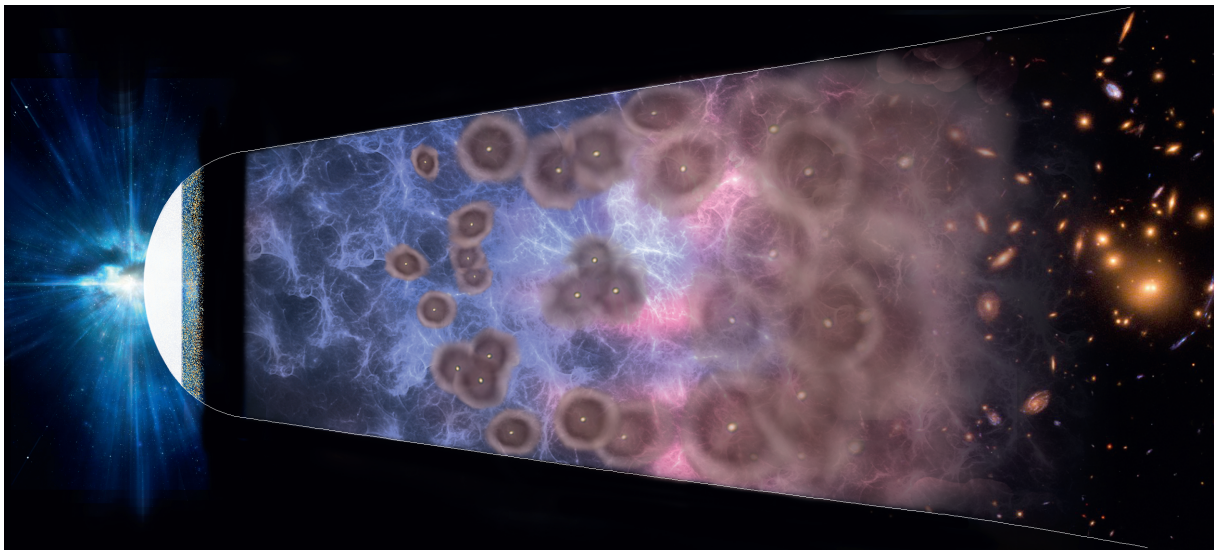

Figure 1.2: A visual overview of the main stages in the evolution of the Universe. The white part at the beginning represents the first 370.000 years and displays the epoch of recombination and decoupling. This is followed by the Dark Ages. After a few million years, the first stars were formed which initiated the Epoch of Reionization, where the neutral hydrogen was ionized again by the light coming from the first stars. Image Credit: Delphi framework (ERC:717001)

This reionisation greatly influenced the formation and further evolution of galaxies and it is therefore of great importance that we observe galaxies at this stage. The Epoch of Reionization is thought to start at around $z \sim 15$ and to be fully complete at $z \sim 6$ (Dunlop, 2013; Sun & Furlanetto, 2016; Fan et al., 2006; Mason et al., 2018). One way of determining if a galaxy is still ionizing the ISM is by looking for the Lyman break. As said before, in the Epoch of Reionization, the Universe was opaque for hydrogen-ionizing photons. The energy necessary to ionize hydrogen is 13.6 eV. The wavelength of the photons corresponding to this energy is $\leq$ 912Å. These are photons that ionise the interstellar medium(ISM). If a galaxy is still ionizing the ISM, the vast majority of these photons will be absorbed within the galaxy and thus cannot escape the galaxy. Hence these photons will not be visible in the spectrum. This process creates a cut-off in the spectrum which is commonly referred to as the Lyman break. I will go further in detail about the Lyman break and other observables in section 1.3.

1.3 Observing Early Galaxies

There are currently multiple techniques for detecting high redshift galaxies (Dunlop, 2013). Two very effective methods depend on neutral hydrogen. One of these methods is by using the previously mentioned Lyman break, which allows for studying the stellar population. Since the cut-off always happens at 912Å in the restframe, it is possible to determine its redshift by looking at how much the cut-off has shifted. The other method uses the Lyman α emission of a galaxy, which is produced by excited neutral hydrogen. This excitation is caused by the young stars.

One of the main drawbacks of these two methods is that they are very biased towards galaxies with young stellar populations since these methods depend heavily on the excessive production of

ultraviolet light. To combat this bias, there is also a method which focuses on the lower energy end of the spectrum. This method observes the Balmer break, which happens at $\lambda_{rest} = 3646$Å(see Figure 1.3). At redshifts ≥ 5 this break is not visible with ground-based observatories and is hence mostly observed by Spitzer. Unfortunately, only a few high redshift galaxies have been found using this method. It could be that galaxies in the early Universe just have much more young stars for the Balmer method to be more effective at observing them. It could also be that Spitzer is not advanced enough to observe the Balmer break at these high redshifts. The James Webb Space Telescope (JWST) could perhaps resolve this issue due to increased sensitivity and clarity. (Dunlop, 2013).

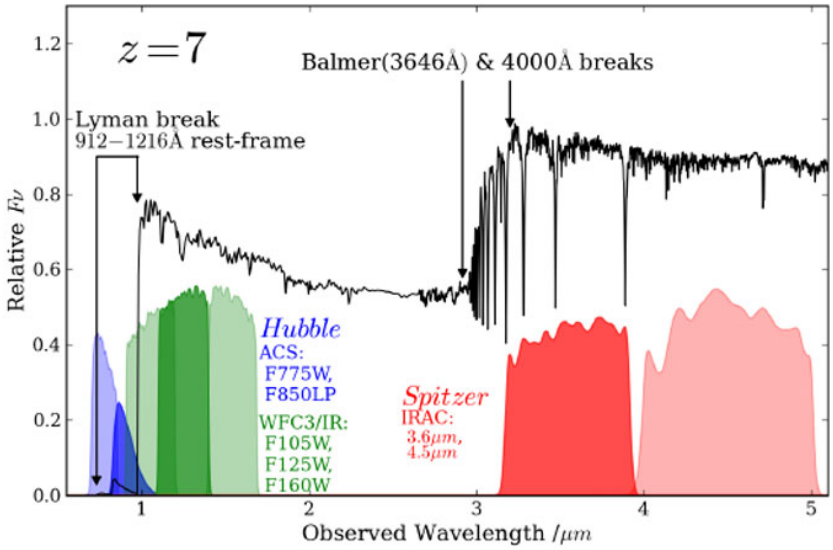

Figure 1.3: This image displays the Lyman break and Balmer break, which happen at 912Å and 3646Å respectively in the restframe. These breaks are caused by the ionization of hydrogen. The Lyman break is caused by ionisation from the ground state and the Balmer break is by ionisation from the second energy level. These breaks are useful for determining the range of the redshift of a galaxy, as they are very recognisable in its spectrum. This spectrum is already at redshift 7. The blue region represents the window in which the ACS camera on the Hubble space telescope (HST) can observe. The green part is also observed by the HST, but then by the WFC3/IR camera. And lastly, the red part can be observed by the Spitzer space telescope.Image credit: Dunlop (2013)

Some methods, however, do not depend on hydrogen. One of these methods is to observe the thermal dust emission. Thanks to the Atacama Large Millimetre Array (ALMA), this method has been able to detect thermal dust emissions. In a large program called the Reionization Era Bright Emission Line Survey (REBELS), 40 of the brightest galaxies at $z \geq 6.5$ over a 7 deg^2 area are being studied, where they scan for bright ISM cooling lines, such as [COII] 158μm and [OIII] 88μm (Dayal et al., 2022; Sommovigo et al., 2022) In these early stages of the Universe, there were little to no metals to produce the dust emission spectrum. So it will mostly be constrained to more moderate redshifts. However, by observing this emission spectrum, a more complete image of galaxy evolution can be obtained, since dust absorbs UV and optical photons (Dayal et al., 2022). This method is also still quite young but has already observed a galaxy at $z = 5.3$

by Riechers et al. (2010) using the CO line.

Another technique is observing the accretion of central supermassive black holes (Dunlop, 2013; Carilli et al., 2010). They produce very strong active nuclear emissions. Unfortunately, this strong emission overpowers the rest of the spectrum, which makes it very hard to detect, let alone study, the stellar population of the host galaxy (Targett et al., 2012). This limits the use of this technique in the study of early galaxy evolution.

Another fairly new method is observing Gamma-Ray Bursts(GRB) (Dunlop, 2013; Gehrels et al., 2004). These are very luminous events, potentially caused by supernovae of low-metallicity, massive stars. Due to their luminosity, they are still very visible at redshifts > 8. Unfortunately, this method does not provide much information about the host galaxy yet. But future developments might alleviate this problem (Dunlop, 2013).

Lastly, there is also some development in using CO molecular lines to observe high redshift galaxies (Carilli et al., 2010; Vallini et al., 2018). This would be able with ALMA, but it still needs further research to become as well used as the hydrogen-based methods.

These observations can tell us a lot about the properties of these galaxies. One of the most important properties is the stellar mass, which can be linked to the star-formation rates(SFR) and can provide a comparison to a different model that we currently have on galaxy formation. Dunlop (2013) points out that there is some debate on what the SFR would look like in early galaxies. Growing evidence suggests that the SFR is more or less constant at earlier times (Eyles et al., 2007; Dunlop, 2013). However, plenty of evidence can be found for other models on the evolution of the SFR (Stark et al., 2009). To say anything conclusive about the stellar evolution of high-redshift galaxies, high-resolution spectroscopic observations are needed as confusion may arise due to dust and nebula extinction, and metallicity.

1.4 The Observed UV luminosity function

The luminosity function(LF) is one of the key observables of the galaxy population at a given redshift. It is defined as the number of objects per unit comoving volume per luminosity,

$$\delta N = \Phi(L)\delta L \delta V$$

the luminosity function per luminosity is often defined by the Schechter function (Schechter, 1976),

$$\frac{dN}{dV} = \Phi(L)dL = \phi^* \left(\frac{L}{L^*}\right)^{\alpha} e^{\frac{L}{L^*}} d\left(\frac{L}{L^*}\right) \tag{1.1}$$

where ϕ^* is a normalisation factor, L^* is the characteristic luminosity of the "knee" and α is the slope of the faint end of the luminosity function. The luminosity function (LF) is used to predict the luminosity density of the Universe, galaxy number counts and the redshift distribution of galaxies. Additionally, it is a good tracer for the mass of galaxies if you observe it in the K-band of the HST for $4 < z < 13$. This is because a lot of stars with long-lived progenitors. However, the UV will be of interest in this paper. This wavelength regime is closely tied to the star formation rate of galaxies. A special interest will be taken in the wavelength $\lambda = 1500$Å. This is a UV wavelength and is chosen because this is the centre wavelength of the observation

window that the HST has in the UV. The relation that equation 1.1 would predict can be seen in Figure 2.2.

Unfortunately, this is not what we observe in the Universe. It fits the medium to high luminosity end of the function, but the low luminosity end does not match. At the low luminosity end, a lot fewer galaxies are observed. This means that ΛCDM predicts a lot of tiny galaxies and relatively few big galaxies. But if one looks at the Local Group we already do not observe as many dwarf galaxies as one might expect from equation 1.1.

Why would there be considerably fewer small galaxies in the Universe than what ΛCDM predicts? One explanation might be that these galaxies are not observed but that they are there. This is not a likely explanation though, as the vast majority should be smaller galaxies. Saying that they are too faint to observe is also not very likely since we still observe the same decline with the increasing sensitivity of ALMA. If they were too faint to observe, we would see an increase of these low luminosity halos with increasing sensitivity. However, the decline persists. Hence it seems more likely that fewer small galaxies/halos are something inherent to the Universe.

Another explanation is that the ΛCDM model is not correct, but that in reality, dark matter is not cold but warm or even hot. This does not mean that it has a physical temperature, but that the dark matter particles have some energy or thermal velocity. This would allow for the dark matter particles to escape the potential wells described in section 1.1, which would result in a smoother Universe where small halos never form. Hence one would observe fewer smaller galaxies. Dziouba (2022) has written a thesis on this explanation for this decrease.

The explanation that will be considered in this work however is that some processes in the Universe would lower the star formation efficiency in some way. This would not inhibit the formation of small halos but would result in fainter low mass halos. How this explanation is evaluated can be seen in the next sections.

Chapter 2

Theoretical Framework

In the majority of this thesis, the assumption was made that the baryonic matter content in a dark matter halo reflects the cosmological abundances in the Universe. This is a basic and fair assumption if the halo falls within a high mass range ($M_h \geq 10^{10} M_\odot$). However, as explained in section 1.4, this does not hold at the low luminosity end.

Therefore, it is important to know how one describes the population of galaxies and where the models, that seem to disagree with the data, come from. The main function that we use to study galaxy populations is the halo mass function. Unfortunately, it is not possible to observe the mass directly. It is, however, possible to observe their luminosities, hence the observations give the luminosity function. In section 2.1, I will discuss the analytical model used for the calculations that are used as a basis for this thesis. In section 2.2, an explanation will follow on how to convert the Halo Mass Function into the Luminosity function.

Lastly, an overview will be given of one of the explanations of why the implied baryonic matter content of a galaxy is lower than expected by the model used in section 2.2. This process is supernovae feedback and will be discussed in section 2.3.

2.1 Dark Matter Halo Mass Function

As previously mentioned, dark matter form halos and in these halos galaxies form. It is, therefore, useful to be able to describe the evolution of these dark matter halos over the lifetime of the Universe. One of the most widely used models of describing these halos is the Halo Mass Function(HMF). This function indicates the number density per comoving volume of halos that have a specific mass. The exact form of the HMF depends on the cosmology that one assumes. If one assumes the ΛCDM model, as is done in this thesis, the number density of halos goes up as the mass of the halos decreases.

In earlier analysis, the Schechter function was used to calculate the HMF,

$$f(\sigma) = \sqrt{\frac{2}{\pi}} exp\left(-\frac{\delta_c^2}{2\sigma^2}\right) \tag{2.1}$$

where $f(\sigma)$ is the fitting function, δ_c is the critical overdensity for spherical collapse and σ is the mass variance (Murray et al., 2013).

However, later was found that this equation was a good approximation, but did not describe the behaviour very well. It was predicting too many low-mass halos and too few high-mass halos. This was corrected by considering ellipsoidal gravitational collapse rather than spherical (Sheth et al., 2001). This changed the $f(\sigma)$ term a little.

Additionally, this version did not take redshift into account. This was corrected by including a mass variance, $\sigma(M, z)$, which also depends on redshift. The behaviour of $\sigma(M, z)$ depends strongly on the growth factor. The growth factor is a parameter that defines the amplitude of the fluctuations in large scale structures (Hamilton, 2001). The growth factor in the used model by Murray et al. (2013) is given by

$$d(z) = \frac{D^+(z)}{D^+(z=0)} \tag{2.2}$$

where $D^+(z)$ is

$$D^+(z) = \frac{5\Omega_m}{2} \frac{H(z)}{H_0} \int_z^\infty \frac{(1+z'')dz}{(H(z')/H_0)^3}$$

The second term in equation 2.1 is the ratio between the present day Hubble parameter and the Hubble parameter at redshift z

$$H(z) = H_0 \sqrt{\Omega_m (1+z)^3 + (1-\Omega_m}$$

Putting all of this together leads to the expression used by Murray et al. (2013):

$$\frac{dn}{dlnM} = M \cdot \frac{\rho_0}{M^2} f(\sigma) \left| \frac{dln\sigma}{dlnM} \right| \tag{2.3}$$

This is the equation implemented in the module used for the simulations, which can be found on `https://github.com/steven-murray/HMF`. This module allows for retrieving simulations of the HMF from the previously described conditions. A more in-depth explanation of the code and how to use it can be found in Murray et al. (2013). This code also allows for simulations for different models of dark matter, such as warm dark matter but was not used in this thesis.

The simulations used in this work were provided by Prof Dr P. Dayal and were generated at redshifts between $4 - 14$. The results of these simulations are displayed in Figure. 2.1

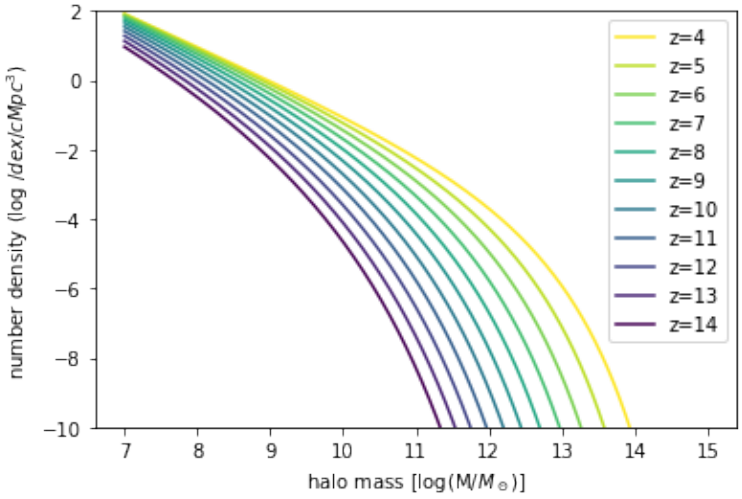

Figure 2.1: The halo mass function at redshifts 4-14 can be seen in the above graph. These are a raw plot of the simulations that were given at the stars of this research. The model used to obtain these simulations is CDM.

These simulations are used throughout this paper as a basis for the calculations to attain the luminosity function.

2.2 Ultraviolet Luminosity Function

The supplied simulations give the relation between the dark matter halo mass and the number density function and are based on the work by Murray et al. (2013). Unfortunately, the halo mass is not observed, instead, the luminosity of a galaxy is observed. To compare the simulations and the observations, a conversion between halo mass and luminosity is needed. A basic model for this is given by Pacucci et al. (2022). The steps to arrive at this conversion are quite simple.

First, we convert the halo mass, M_h, to gas mass,M_g. This is done by taking the ratio of baryonic matter density to dark matter density and multiplying it with M_h,

$$M_g = \frac{\Omega_b}{\Omega_{dm}} M_h$$

Next, we obtain the stellar mass, M_*, by multiplying M_g by the star formation efficiency, f

$$M_* = f M_g.$$

This will indicate the number of young stars, which have the peak of their bolometric luminosity in the UV. Hence these will be the dominant producers of photons at λ_{1500}. Finally, the conversion from stellar mass can be made to luminosity. This is done by multiplying it by the specific luminosity, L_{1500}

$$L = L_{1500} M_*.$$

Putting all these equations together, we obtain the equation specified in Pacucci et al. (2022),

$$L = \frac{\Omega_b}{\Omega_{dm}} f L_{1500} M_H \tag{2.4}$$

Now that the simulations are converted into luminosity, they can be almost compared to the observations. Most observations are given in absolute magnitude. This is very convenient since the redshift dependence drops out for absolute magnitude. This can be seen when one uses the following equations for absolute and apparent magnitude respectively,

$$M = m - 5log\left(\frac{1+z}{10pc}\right),$$

$$m_{AB} = -2.5log(F)$$

where

$$F = \frac{L}{4\pi(1+z)^2}.$$

If one substitutes the given equation for the apparent magnitude in the equation for the absolute magnitude and corrects for the units, equation 2.5 is obtained,

$$M = -2.5log\left(\frac{L\lambda^2}{4\pi c \cdot 3631\text{Jy} \cdot 100\text{pc}^2}\right) \tag{2.5}$$

This equation together with equation 2.4 will allow the simulations to be compared to the observations, which will be explained later in this paper. When using the star formation efficiencies from Pacucci et al. (2022) and the cosmological densities from the ΛCDM model we retrieve the UV LF displayed in Figure 2.2

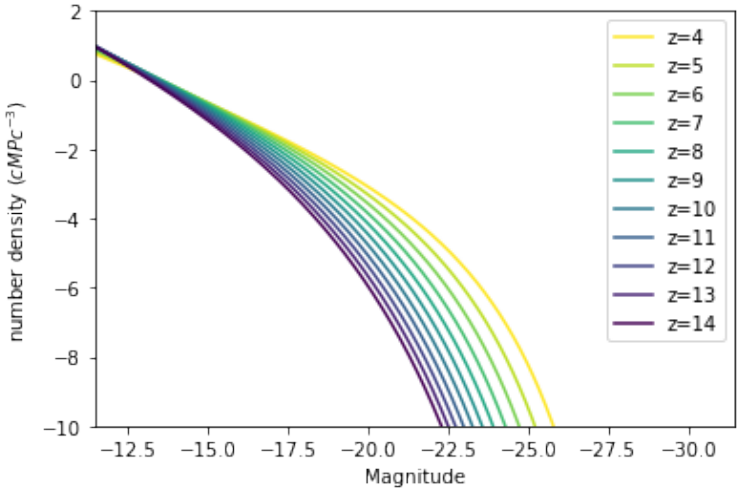

Figure 2.2: This graph displays the luminosity function obtained from the simulated halo mass function displayed in Figure 2.1. It indicated the number density of galaxies as a function of magnitude. This conversion comes from converting the Halo Mass to luminosity via the equations given in Pacucci et al. (2022). Afterwards, the luminosity was converted to magnitude using equation 2.5.

2.3 Supernovae Feedback

As said before, some processes can influence the baryonic matter content and in turn affect the star formation efficiency of a galaxy. All processes that affect the star formation efficiency are called feedback. Here, I will focus mainly on supernovae feedback; feedback caused by a supernova. During a supernova, an immense shock wave is created. This could cause shock-heating, molecule dissociation, photo-evaporation and ejection of gas out of the halo (Dayal et al., 2014). These are all processes that quench star formation.

For a star to form, a cold cloud is needed which can gravitationally collapse. If this cloud is heated, the star formation efficiency will go down. If the density of the gas is too low, the collapse will be slowed down and hence the star formation efficiency will go down.

Here the focus will mainly be on the ejection of gas from the halo. Mass ejection can be caused by a supernova. These supernovae typically have an energy of $E_{SN} = 10^{51}$ erg, which is released to the ISM (Dayal et al., 2014). This results in the surroundings being heated up and pushed away in a shockwave(Benson et al., 2003). The shock heating will lessen the star formation efficiency a bit, but the ejection will actually "starve" the galaxy of material to form new stars (Dayal et al., 2014). To be able to continue to form stars, the halo has to accrete baryonic matter again or have to merge with another halo that has baryonic matter in it. If it fails to do this, the halo has much fewer stars in it than what one would expect if you look exclusively at its halo mass. This lack of stars would make the halo appear to be fainter.

For gas ejection to take place, the energy released by the supernova must be bigger than the energy required to release all the ISM gas, $E_{SN} \geq E_{ej}$. How big E_{ej} differs from star to star and can be expressed as (Dayal et al., 2014)

$$E_{ej} = \frac{1}{2} \left[M_{g,i}(z) - M_*(z) \right] v_e^2$$

where $M_{g,i}$ is the gas mass in the halo at redshift z, M_* is the mass in stars at redshift z and v_e is is the escape velocity. How efficient this ejection is depends on multiple factors. Dayal et al. (2014) defined the ejection efficiency, the fraction of gas that has to be converted into stars to expel the rest of the gas, as

$$f_*^{ej} = \frac{v_c^2(z)}{v_c^2(z) + f_w v_s^2} \tag{2.6}$$

where v_c is the rotational velocity of the halo, defined as $v_e = \sqrt{2}v_c$, and f_w is the fraction of the energy released during the supernova explosion that is converted into kinetic energy that drives the shock wave. v_c increases with redshift as $v_c \propto (1+z)^{1/2}$.

From equation 2.6 it can be inferred that galaxies are more efficient at maintaining their gas with increasing redshift. This is due to deeper potential wells at higher redshifts (Dayal et al., 2014).

Additionally, it will take more energy to eject gas from a bigger halo compared to a small halo. The potential well of a less massive halo is shallower than one of a more massive halo. Hence it will be more difficult for matter to escape the potential well, and thus the halo, for more massive halos.

Chapter 3

Methods

3.1 Key Results

In this thesis, data from multiple papers were combined to fit the models. The complete data set was supplied by Prof. Dr. P. Dayal and contained the work of Harikane et al. (2022), Bouwens et al. (2021), Finkelstein et al. (2015), Bowler et al. (2015), Ishigaki et al. (2018), Bowler et al. (2020), Bouwens et al. (2020) and Oesch et al. (2018). Intermediate luminosities ranging from $-22 < M < -18$ were used to fit the star formation efficiency in the next section. This data is more extensive than the data used by Pacucci et al. (2022), with which I will compare my findings. Hence some slight disagreement could arise.

3.2 The Emerging SFE of early galaxies

The data from the observations is given in magnitude versus number density. However, the simulations were in halo mass versus number density. To fit the function to go from halo mass to magnitude, the data luminosities have to be coupled to the simulated halo masses.

At first, this was done by abundance matching, since the number densities mapped one-to-one in the simulations. Hence one observed number density had one observed magnitude, but this number density also had a value for halo mass in the simulations. This value for the halo mass was taken to be the value which belonged to the magnitude because they had the same number density. However, abundance matching has no predictive abilities, hence another method had to be used.

For this alternative method, f was fitted by eye to the data for $-22 < M < -18$. This middle section was chosen since, at magnitudes fainter than -18, the data points start deviating from a Schechter function and become flatter. In this analysis, it is assumed that this is caused by fewer stars being formed in low-mass halos. For magnitudes brighter than -22 it also differs slightly from a Schechter since it seems to steepen there. This is probably caused by dust extinction. Since bigger halos contain more dust, some of the light gets absorbed by the dust making the halo look fainter. Hence the brighter halos are observed as fainter than what they are (Bowler et al., 2015). The intermediate luminosities will therefore give the most reliable fit.

To get an idea if the values retrieved from these two methods are accurate, they were compared with the values obtained in Pacucci et al. (2022). They found a relation between redshift and f that can be nicely summed up by a linear equation:

$$log(f(z)) = 0.125z - 3.435 \tag{3.1}$$

The results of this equation are represented by the green points in Figure 3.1

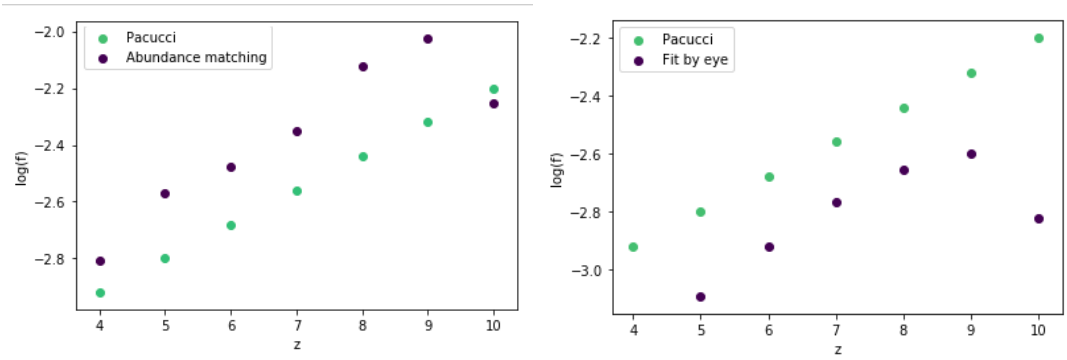

Figure 3.1: This figure displays the evolution of the star-forming efficiency as a function of redshift. The purple points have been retrieved from fitting the luminosity function to the data points. The green points are the values for the star forming efficiency predicted by equation 3.1 by Pacucci et al. (2022), the left image displays log(f) obtained by abundance matching and the right image displays log(f) obtained by fitting the middle section of the LF by eye.

As can be seen in Figure 3.1, the shape of the evolution of $log(f)$ has changed a bit from the results obtained from Pacucci et al. (2022). For the abundance matching method, there is a dip at $z = 10$. This dip is also visible in the right image. Both methods result in a vertical shift of the values for f from Pacucci et al. (2022), but then with a dip at $z = 10$. The absence of a dip in Pacucci et al. (2022) might be caused by an insufficient amount of data at $z = 10$. It might be that they, therefore, ignored the dip since it did not align with the general trend observed at $4 \leq z \leq 9$. It is interesting to note that abundance matching results in an upward shift and the fitting by eye results in a downward shift

Since abundance matching is not the most reliable method for fitting the data and the low luminosity and high luminosity end are taken into consideration, the fitting by eye method was used as a final method to fit the star formation efficiency.

This resulted in a UV LF seen in Figure 3.2. When comparing it to f retrieved from equation 3.1, one sees that the UV LFs agree fairly well. The only UV LF that differs significantly is the UV LF for $z = 10$. It might be that Pacucci et al. (2022) might not have taken $z = 10$ too much into consideration since it has very few data points and differs considerably from the trend obtained from $4 \leq z \leq 9$.

As you can see in Figure 3.2, the resulting f still fits reasonably well but can be improved. In Figure 3.2, the gas fraction inside the halo was taken into account. What if this does not reflect the cosmological abundances predicted by the ΛCDM model? In the next paragraphs, supernovae feedback in the form of gas ejection will be taken into account.

Initial bounds were put in place to create a grid for which the goodness of fit can be calculated for each value on the grid. The two parameters that were fitted are f and ρ_b/ρ_{dm}; the ratio between the baryonic matter density and the dark matter density. Since f is by definition between 0 and 1, these were the initial bounds put in place for f. For ρ_b/ρ_{dm} and upper limit of $\frac{\Omega_b}{\Omega_{dm}}$ was chosen, since if we have ejection from the halo the maximum ratio between the baryonic matter density and the dark matter density is the ratio predicted by the ΛCDM model. As a lower limit for ρ_b/ρ_{dm} 0 was chosen, this would imply that the mass ejection would be so efficient that it would blow away all the gas in the halo.

These values were then one by one put into equation 2.4 and tested on how good they fit the data points as a whole. For this model, it was assumed that f and ρ_b/ρ_{dm} stayed constant

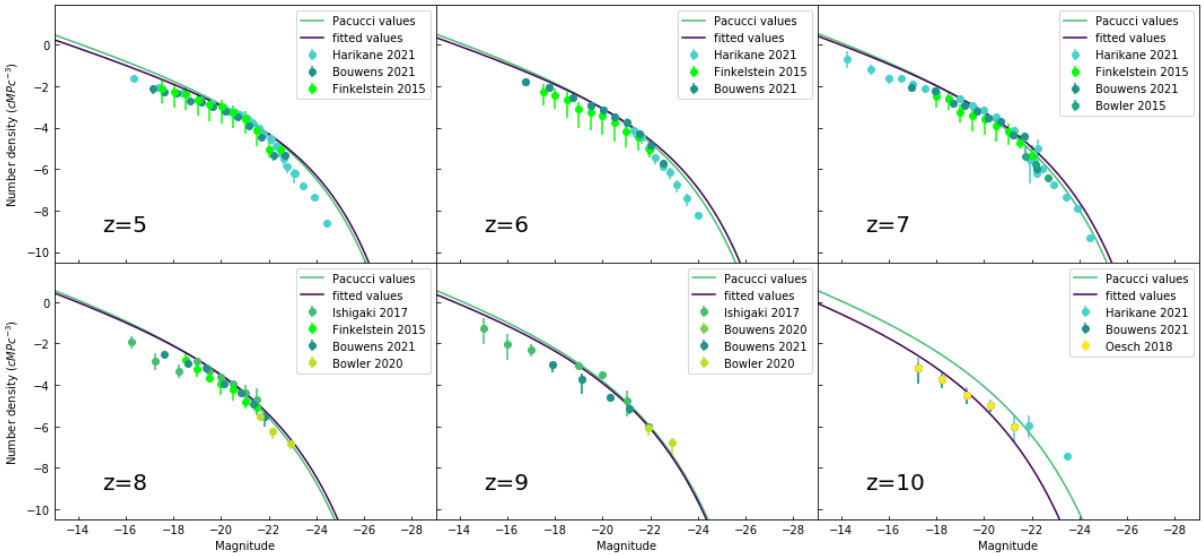

Figure 3.2: The above figure displays the data from Harikane et al. (2022), Bouwens et al. (2021), Finkelstein et al. (2015), Bowler et al. (2015), Ishigaki et al. (2018), Bowler et al. (2020), Bouwens et al. (2020) and Oesch et al. (2018) together with two simulated luminosity functions per redshift. The purple line indicates the simulated values from Pacucci et al. (2022) which can be seen in Figure 2.2. The green line shows the values from the same simulations, but with the fitted values for the star forming efficiency which are plotter in Figure 3.1

overall M_h at a specific redshift.

To test the goodness of fit for each individual set of values on the grid, the χ^2 method was used. Specifically the χ^2 module from `scipy.stats`. The values plotted in Figure 3.3 is χ^2 test statistics, which is defined as

$$\chi^2 = \sum_{i=1}^{k} \frac{(O_i - M_i)^2}{M_i} \tag{3.2}$$

where O_i is the observed magnitude and M_i is the magnitude as predicted by the model. Because we are dealing with quite bright objects, the magnitudes are negative and hence the χ^2 value is also negative. If the value is closer to zero, the fit is good and the further away from zero it is the worse the fit.

Since we assume that f and ρ_b/ρ_{dm} do not change as a function of halo mass, there is one constant for $f \cdot \rho_b/\rho_{dm}$ that will give an optimal fit to the data. Hence a hyperbolic shape is expected for the colour map. This is also exactly what can be seen in Figure 3.3.

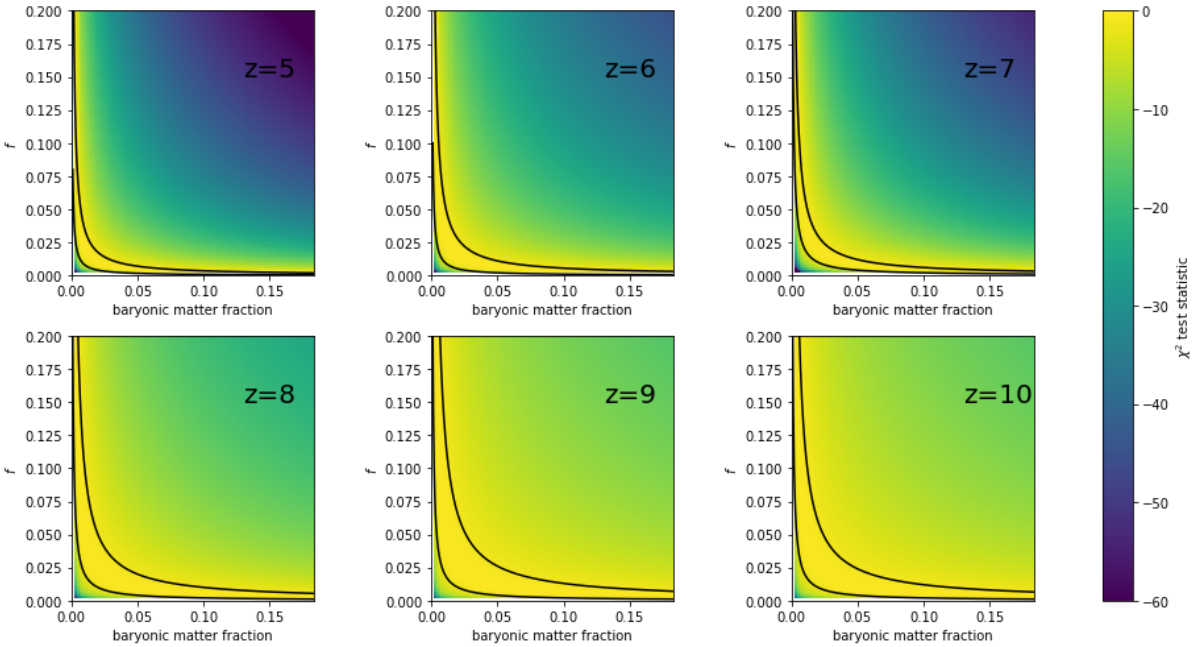

Figure 3.3: This figure displays how good a certain combination of f and ρ_b/ρ_{dm} fits the data at a specific redshift. These values are the χ^2test statistic.The black lines indicate the interval where the the χ^2 test statistic was higher than -1.

One can see that the product of ρ_b/ρ_{dm} and f gets more uncertain at higher redshifts. This is probably due to an increase in the size of the error bars and a decrease in the number of data points. Hence a tighter constraint can be put on the product of ρ_b/ρ_{dm} and f at lower redshifts with the current data. The table displayed in Appendix A lists the upper and lower bound that are displayed in Figure 3.3. If one applies these bounds in equation 2.4, one gets the UV LF's displayed in Figure 3.4

It is more likely that the true value lies within the horizontal part of the best fit since such a high star formation efficiency is not very likely nor is such a low baryonic matter fraction. As a rough estimate for f, the fitted values for f displayed in Figure 3.2 were used. The lower limit for ρ_b/ρ_{dm} was defined as the point where this star formation efficiency crossed the boundaries of Figure 3.3. As an upper limit the predictions from the ΛCDM model were used, so the cosmological abundances. The area enclosed by these limits and the boundaries displayed in Figure 3.3 is then the constraints put on ρ_b/ρ_{dm} and f. The enclosed area is displayed in Figure 3.5.

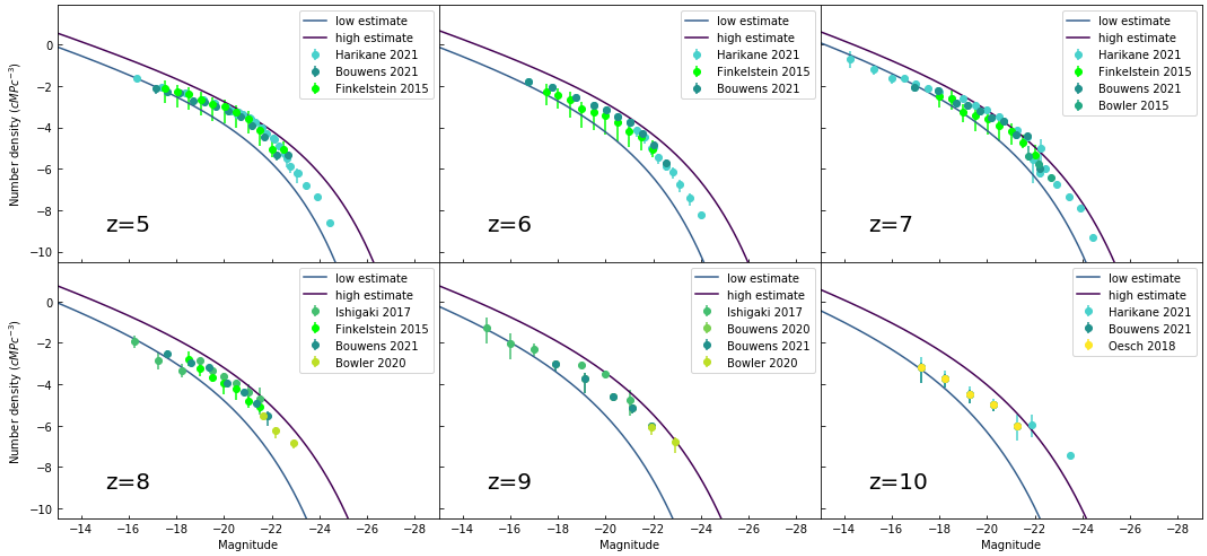

Figure 3.4: This figure displays the data from citeharikane2022search, Bouwens et al. (2021), Finkelstein et al. (2015), Bowler et al. (2015), Ishigaki et al. (2018), Bowler et al. (2020), Bouwens et al. (2020) and Oesch et al. (2018). The purple and blue line indicate the high and low estimate for the product of the star formation efficiency and ratio between baryonic matter and adark matter respectively. These estimates were obtained from Figure 3.3

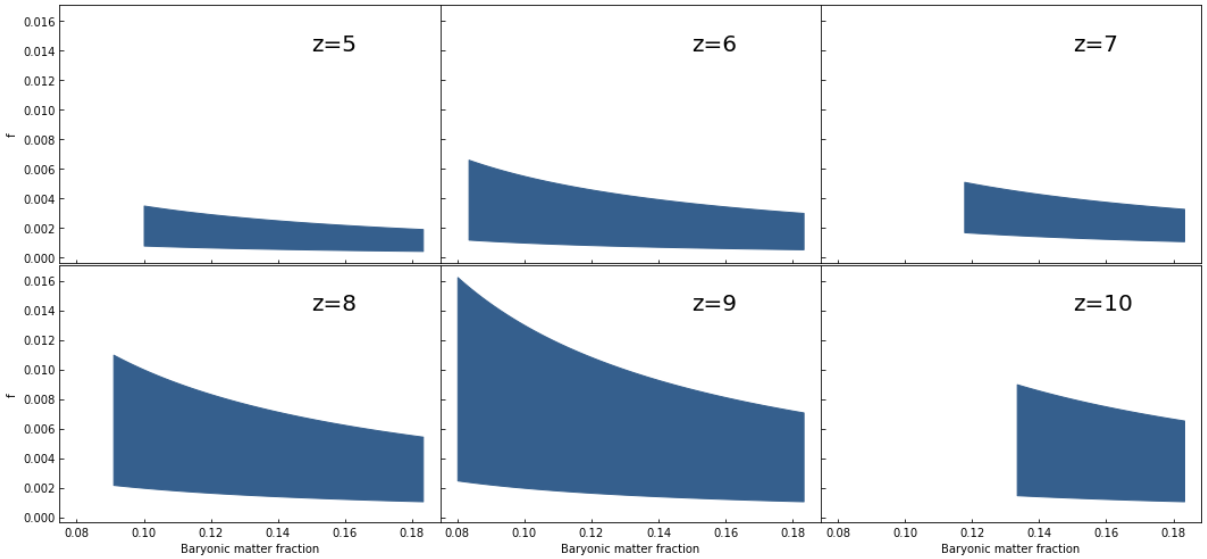

Figure 3.5: The shaded areas illustrate the boundaries within which the star formation efficiency and the ratio between baryonic matter and dark matter must lay according to this analysis based on Figure 3.3.

Chapter 4

Discussion and Conclusion

The goal of this thesis was to put constraints on the star formation efficiency and the density ratio of baryonic matter and dark matter in halos at different redshifts. To do this, the assumption was made that these parameters only change as a function of redshift. How well the constraints fit the data can be seen in Figure 3.4 and the area in which these parameters must lay is displayed in Figure 3.5.

The chosen bounds encapsulate the data quite well. The only data set that did not fit that well was the data at $z \sim 10$. This is probably mainly caused by the lack of data points which might not give the clearest image of the galaxy population at this redshift. It is difficult to observe at higher redshifts, hence the observations become sparser when the redshift increases.

What is interesting to note is that the lower bound generally fits the low luminosity end pretty well, while the higher bound fits the middle region of the luminosity function better. This was to be expected since, as described earlier, the low luminosity end has lower number densities than expected. Hence a lower value of the product of ρ_b/ρ_{dm} and f is better fitted.

Another interesting finding was that at redshifts 5, 6 and 7, the high luminosity end was also better fitted by the lower bound than the upper bound. This might be caused due to dust attenuation, which is more influential at higher mass halo's (Pacucci et al., 2022). The sudden decline at the high luminosity end is less pronounced at redshifts 8, 9 and 10. This might be due to a lack of dust at these redshifts. These redshifts reside in the Epoch of Reionization when the first stars have just died. It is very well possible that the ISM is not enriched enough yet to have sufficient dust that the dust significantly influences the magnitude of the galaxy in the UV.

Even when altering ρ_b/ρ_{dm} and f, the discrepancy between the low end of the LF and the middle part persists. It is therefore likely that the initial assumption, that ρ_b/ρ_{dm} stays constant over all M_h, was incorrect. It is hence likely that f depend on M_h as suggested by Dayal et al. (2015). ρ_b/ρ_{dm} is likely much lower in low mass halos since the ejection of matter by supernovae is more efficient in those halos as described in section 2.3.

For future work it is advised to look into this prospect and study how ρ_b/ρ_{dm} and/or f depend on M_h. Dayal et al. (2015) suggests a dependence of $f \propto 2^{-1/M_h}$. However, a more complicated relation is suggested by Sun & Furlanetto (2016). Hence further research in determining the exact relation between f and M_h, will be beneficial in deepening the understanding of the evolution of galaxies.

Something that could be improved in further research is the statistical analysis of the data. A full statistical analysis was beyond the purview of this thesis. A follow-up study would do well

to take the degrees of freedom into account for the determination of a better boundary value of the χ^2 test statistic. This would give the constraints more statistical significance and give somewhat of a confidence interval on them.

Additionally, an expansion of the current data set would be welcome. The data at $z \sim 7$ appears to be sufficient at the extreme of the UV LF, but especially at $z \geq 8$ the data gets a bit sparse. The data at $z = 5$ and $z = 6$ also does not extend that far in the low luminosity end, which would be very helpful since this end has a major influence in the debate about the shape of the UV LF. Powerful telescopes, such as the JWST and ALMA, are necessary to probe further into the Universe at lower luminosities. This is crucial if we want to understand the UV LF better and put better constraints on ρ_b/ρ_{dm} and f.

With the current data available the ΛCDM model is still viable if combined supernovae feedback. This phenomenological model has to contain the constraints given in Table 4.1.

z	f_{min}	f_{max}	$(\rho_b/\rho_{dm})_{min}$	$(\rho_b/\rho_{dm})_{max}$
5	4.21e-04	3.50e-03	0.100	0.183
6	5.26e-04	6.60e-03	0.083	0.183
7	1.05e-03	5.10e-03	0.118	0.183
8	1.05e-03	1.10e-02	0.091	0.183
9	1.05e-03	1.63e-02	0.080	0.183
10	1.05e-03	9.00e-03	0.133	0.183

Table 4.1: This table displays the upper and lower constraints on the star formation efficiency and the ratio between baryonic matter and dark matter at redshifts 5-10, based on data by Harikane et al. (2022), Bouwens et al. (2021), Finkelstein et al. (2015), Bowler et al. (2015), Ishigaki et al. (2018), Bowler et al. (2020), Bouwens et al. (2020) and Oesch et al. (2018).

As is displayed in Figure 3.4, the boundaries fit quite well. Unfortunately, the current data is not conclusive enough to rule out other explanations such as Warm Dark Matter. The thesis by Dziouba (2022) also analyses this problem but then assumes a WDM paradigm. She concluded that the 3 keV variant of WDM fitted the data better than 1.5 keV, but that there was not a 100% agreement between the data and the model. Hence Dziouba (2022) could not conclusively confirm that WDM is the explanation for the decline at the low luminosity end of the UV LF.

From an examination of Figures 10 to 15 in Dziouba (2022), I think that a phenomenological model of CDM for galaxy evolution might have more potential since the overall shape of the WDM model did not seem to fit the shape of the observed UV LF very well. If one were to adopt a halo mass-dependent f, I think the overall shape of the simulations might provide a better fit than WDM.

Chapter 5

Acknowledgements

First and foremost I would like to thank my supervisor Prof Dr Pratika Dayal for allowing me to do this project and for her support and feedback throughout my research. Additionally, I would like to thank my second reader, Prof Dr Karina Caputi for taking the effort to read my thesis.

I would also like to thank the members of Pratika's research group; Jonas Bremer, Valentin Mauerhofer, Laurent Legrand, Maxime Trebitsch, Anne Hutter and Chris Böttner. For giving feedback on my first draft and helping with concepts that I struggled with.

Lastly, I would also like to thank my friends and fellow students for the mental support, advice during the project and feedback on my thesis. I would especially like to thank Maria Dziouba, whose project ran parallel to mine and with whom I could discuss problems I encountered during my research.

Bibliography

Aghanim N., et al., 2020, Astronomy & Astrophysics, 641, A6

Benson A., Bower R., Frenk C., Lacey C. G., Baugh C., Cole S., 2003, The Astrophysical Journal, 599, 38

Bouwens R., et al., 2020, The Astrophysical Journal, 902, 112

Bouwens R., et al., 2021, The Astronomical Journal, 162, 47

Bowler R., et al., 2015, Monthly Notices of the Royal Astronomical Society, 452, 1817

Bowler R., Jarvis M., Dunlop J., McLure R., McLeod D., Adams N., Milvang-Jensen B., McCracken H., 2020, Monthly Notices of the Royal Astronomical Society, 493, 2059

Bullock J. S., Boylan-Kolchin M., 2017, arXiv preprint arXiv:1707.04256

Carilli C., et al., 2010, The Astrophysical Journal, 714, 834

Dayal P., Ferrara A., 2018, Physics Reports, 780, 1

Dayal P., Ferrara A., Dunlop J. S., Pacucci F., 2014, Monthly Notices of the Royal Astronomical Society, 445, 2545

Dayal P., Mesinger A., Pacucci F., 2015, The Astrophysical Journal, 806, 67

Dayal P., et al., 2022, MNRAS, 512, 989

Dunlop J. S., 2013, in , The First Galaxies. Springer, pp 223–292

Dziouba M., 2022, Modeling Early Galaxy Evolution in Warm Dark Matter Cosmologies

Eyles L. P., Bunker A. J., Ellis R. S., Lacy M., Stanway E. R., Stark D. P., Chiu K., 2007, Monthly Notices of the Royal Astronomical Society, 374, 910

Fan X., et al., 2006, The Astronomical Journal, 132, 117

Finkelstein S. L., et al., 2015, The Astrophysical Journal, 810, 71

Gehrels N., et al., 2004, The Astrophysical Journal, 611, 1005

Hamilton A., 2001, Monthly Notices of the Royal Astronomical Society, 322, 419

Harikane Y., et al., 2022, The Astrophysical Journal, 929, 1

Ishigaki M., Kawamata R., Ouchi M., Oguri M., Shimasaku K., Ono Y., 2018, The Astrophysical Journal, 854, 73

Koppelman H., 2020, The Galactic halo: formation history and dynamics

Libeskind N. I., Di Cintio A., Knebe A., Yepes G., Gottlöber S., Steinmetz M., Hoffman Y., Martinez-Vaquero L. A., 2013, Publications of the Astronomical Society of Australia, 30

Maoz D., 2016, Astrophysics in a Nutshell

Mason C. A., Treu T., Dijkstra M., Mesinger A., Trenti M., Pentericci L., De Barros S., Vanzella E., 2018, The Astrophysical Journal, 856, 2

Murray S. G., Power C., Robotham A. S., 2013, Astronomy and Computing, 3, 23

Oesch P., Bouwens R., Illingworth G., Labbé I., Stefanon M., 2018, The Astrophysical Journal, 855, 105

Pacucci F., Dayal P., Harikane Y., Inoue A. K., Loeb A., 2022, arXiv preprint arXiv:2201.00823

Riechers D. A., et al., 2010, The Astrophysical Journal Letters, 720, L131

Ryden B., 2017, Introduction to cosmology. Cambridge University Press

Schechter P., 1976, The Astrophysical Journal, 203, 297

Sheth R. K., Mo H., Tormen G., 2001, Monthly Notices of the Royal Astronomical Society, 323, 1

Sommovigo L., et al., 2022, MNRAS, 513, 3122

Stark D. P., Ellis R. S., Bunker A., Bundy K., Targett T., Benson A., Lacy M., 2009, The Astrophysical Journal, 697, 1493

Sun G., Furlanetto S. R., 2016, Monthly Notices of the Royal Astronomical Society, 460, 417

Tanabashi M., et al., 2018, Review of Particle Physics: particle data groups

Targett T. A., Dunlop J. S., McLure R. J., 2012, Monthly Notices of the Royal Astronomical Society, 420, 3621

Vallini L., Pallottini A., Ferrara A., Gallerani S., Sobacchi E., Behrens C., 2018, Monthly Notices of the Royal Astronomical Society, 473, 271

Wechsler R. H., Tinker J. L., 2018, Annual Review of Astronomy and Astrophysics, 56, 435

Zaroubi S., 2013, The First Galaxies, pp 45–101

Zwicky F., 1933, Helvetica Physica Acta, 6, 110

Appendix A

Upper and Lower Bounds

Redshift	Lower Bound	Upper Bound
5	$8 \cdot 10^{-5}$	$3.5 \cdot 10^{-4}$
6	$1 \cdot 10^{-4}$	$5.5 \cdot 10^{-4}$
7	$2 \cdot 10^{-4}$	$6 \cdot 10^{-4}$
8	$2 \cdot 10^{-4}$	$1 \cdot 10^{-3}$
9	$2 \cdot 10^{-4}$	$1.3 \cdot 10^{-3}$
10	$2 \cdot 10^{-4}$	$1.2 \cdot 10^{-3}$

Table A.1: This table displays the upper and lower bound for the best fitting product of f and ρ_b/ρ_{dm}. This was fitted to the data set displayed in Figure 3.2 using equation 2.4.

Appendix B

Code

```
#!/usr/bin/env python
# coding: utf-8

# In[1]:


import numpy as np
from sys import argv
import pandas as pd
# plotting
import matplotlib.pyplot as plt
import matplotlib.cm as cm
import matplotlib as mpl
from matplotlib.colors import Normalize
# constants and units
from astropy.constants import L_sun, M_sun, c
import astropy.units as u
from math import log10, pi
# curvefitting and statistics
from scipy.optimize import curve_fit
from scipy.interpolate import interp1d
from scipy.stats import chisquare


# In[3]:


#importing data
dat10 = np.loadtxt('hmf10.01.dat')
dat11 = np.loadtxt('hmf11.01.dat')
dat12 = np.loadtxt('hmf12.01.dat')
dat13 = np.loadtxt('hmf13.01.dat')
dat14 = np.loadtxt('hmf14.01.dat')
dat4 = np.loadtxt('hmf4.01.dat')
dat5 = np.loadtxt('hmf5.01.dat')
```

```
dat6 = np.loadtxt('hmf6.01.dat')
dat7 = np.loadtxt('hmf7.01.dat')
dat8 = np.loadtxt('hmf8.01.dat')
dat9 = np.loadtxt('hmf9.01.dat')

mass = [dat4[:,0],dat5[:,0],dat6[:,0],dat7[:,0],dat8[:,0], dat9[:,0], dat10[:,0]
        , dat11[:,0], dat12[:,0], dat13[:,0], dat14[:,0]]
numd = [dat4[:,1],dat5[:,1],dat6[:,1],dat7[:,1],dat8[:,1], dat9[:,1], dat10[:,1]
        , dat11[:,1], dat12[:,1], dat13[:,1], dat14[:,1]]

CB_color_cycle = ['#fde725', '#bddf26', '#7ad151',
                  '#44bf70', '#22a884', '#21918c',
                  '#2a788e', '#355f8d', '#414487',
                  '#482475', '#440154']

for i in range(len(mass)):
    plt.plot(mass[i], numd[i], color=CB_color_cycle[i], label ='z={}'.format(i+4
plt.ylim(-10,2)
plt.xlabel('halo mass [log(M/$M_\odot$)]')
plt.ylabel('number density (log $/dex/cMpc^3$)')
plt.legend()
plt.show()


# In[4]:


def sfe(z):
    '''getting star forming efficiency from equation paper'''
    return 0.12*z-3.4

def SFG(z, m, omb = 0.048):
    '''Halo mass to luminosity for a star forming galaxy using paper f'''
    m = 10**m * M_sun
    f = 10**sfe(z)
    omdm = 0.262
    L1500 = 10**33.07*u.erg/u.s/M_sun/u.Angstrom
    return (f*omb/omdm*m*L1500).cgs

def SFGv(m, f):
    '''Halo mass to luminosity for a star forming galaxy using fitted f, just
    the value for fitting purposes'''
    m = 10**m * M_sun
    frac = 0.048/0.262
    L1500 = 10**33.07*u.erg/u.s/M_sun/u.Angstrom
    return (f*frac*m*L1500).cgs.value

def SFGf(m, f, frac = 0.048/0.262):
```

```
    '''Halo mass to luminosity for a star forming galaxy using fitted f, just
    the value for fitting purposes'''
    m = 10**m * M_sun
    L1500 = 10**33.07*u.erg/u.s/M_sun/u.Angstrom
    return (f*frac*m*L1500).cgs

def mag(L):
    '''Conversion luminosity to magnitude'''
    wavel = 1500*u.Angstrom
    freq = c/wavel
    conv = wavel/freq
    return -2.5*np.log10((L*conv/(4*pi*3631*u.Jansky*100*u.parsec**2)).cgs)


def lum(mag):
    '''conversion magnitude to luminosity'''
    wavel = 1500*u.Angstrom
    freq = c/wavel
    conv = wavel/freq
    return 10**(mag/-2.5)*4*pi*3631*u.Jansky*100*u.parsec**2/conv

def LFtoHMFconv(mag, z):
    """Converts absolute magnitude and redshift into logarithmic halo mass."""
    L1500 = 10**33.07                #erg s-1 Angstrom-1 Solar Mass-1
    omb = 0.048
    omdm = 0.262                     #cosmological nonbaryonic dark matter constant
    pc = 3.086e18                    #cm
    loge = 0.12*z-3.4                #star formation efficiency
    L=2e15/1500*4*np.pi*(10*pc)**2*10**((mag+48.60)/-2.5)  #erg s-2 angstrom-1
    Mh = L*(omdm/omb)/(10**loge)/L1500                     #solar masses
    return np.log10(Mh)


# In[5]:


TBHM = []
for i in range(11):
    TBHM.append(np.trapz(10**numd[i], 10**mass[i]))
r=np.linspace(4, 13 ,11)

plt.plot(r, TBHM, color=CB_color_cycle[5])
plt.ylabel('Total Bound Halo Mass (log $M/ M_\odot$)')
plt.xlabel('z')
plt.yscale('log')
# plt.title('Bound Halo Mass')
plt.show()
```

```
# In[6]:


magsim = []
for i in range(11):
    magsim.append(mag(SFG(i+4, mass[i])))

for i in range(11):
    plt.plot(magsim[i], numd[i], color=CB_color_cycle[i], label='z={}'.format(i+
plt.xlabel('Magnitude')
plt.ylabel('number density ($log cMPc^{-3}$)')
plt.title('Luminosity Function')
plt.ylim(-10,2)
plt.xlim(max(mag(SFG(i+4, mass[i]))), min(mag(SFG(i+4, mass[i]))))
plt.legend()
plt.show()


# In[7]:


x = np.load('UVLF.npz')
data4 = x['4']
data5 = x['5']
data6 = x['6']
data7 = x['7']
data8 = x['8']
data9 = x['9']
data10 = x['10']

#Extracting magnitudes, number densities and lower and upper errors of num. dens
magdat = [data4[:,0], data5[:,0], data6[:,0], data7[:,0], data8[:,0], data9[:,0],
numddat = [data4[:,1], data5[:,1], data6[:,1], data7[:,1], data8[:,1], data9[:,1]
errl = [data4[:,2], data5[:,2], data6[:,2], data7[:,2], data8[:,2], data9[:,2], d
erru = [data4[:,3], data5[:,3], data6[:,3], data7[:,3], data8[:,3], data9[:,3], d


# In[8]:


#z = 5
bouwens5 = np.loadtxt('Pratika_data/LBG_bouwens_uvlf_z5.dat')
fin5 = np.loadtxt('Pratika_data/LBG_finkelstein2015_uvlf_z5.txt')
hari5 = np.loadtxt('Pratika_data/LF_riz_combined_wHubble_z5_harikane2021.dat')

#z = 6
bouwens6 = np.loadtxt('Pratika_data/LBG_bouwens_lbg_uvlf_z6_2021.dat')
```

```
fink6 = np.loadtxt('Pratika_data/LBG_finkelstein2015_uvlf_z6.txt')
hari6 = np.loadtxt('Pratika_data/LF_izy_combined_wHubble_z6_harikane2021.dat')

#z = 7
bouwens7 = np.loadtxt('Pratika_data/LBG_bouwens_lbg_uvlf_z7_2021.dat')
Bowler7 = np.loadtxt('Pratika_data/LBG_bowler_lbg_uvlf_z7.dat')
fink7 = np.loadtxt('Pratika_data/LBG_finkelstein2015_uvlf_z7.txt')
hari7 = np.loadtxt('Pratika_data/LF_zy_combined_wHubble_z7_harikane2021.dat')

#z = 8
Bowler8 = np.loadtxt('Pratika_data/Bowler2020_z8.dat')
fink8 = np.loadtxt('Pratika_data/finkelstein2015_uvlf_z8.txt')
ishi8 = np.loadtxt('Pratika_data/ishigaki2017_uvlf_z8.txt')
bouwens8 = np.loadtxt('Pratika_data/LBG_bouwens_lbg_uvlf_z8_2021.dat')

#z = 9
Bouwens9 = np.loadtxt('Pratika_data/Bouwens2020_z9.dat')
Bowler20_9 = np.loadtxt('Pratika_data/Bowler2020_z9.dat')
ishi9 = np.loadtxt('Pratika_data/ishigaki2017_uvlf_z9.txt')
Bouwenslbg9 = np.loadtxt('Pratika_data/LBG_bouwens_lbg_uvlf_z9_2021.dat')

#z = 10
hari10 = np.loadtxt('Pratika_data/data_UVLF_z10_z13_harikane_2021_use.dat')
bouwens10 = np.loadtxt('Pratika_data/LBG_bouwens_lbg_uvlf_z10_2021.dat')
oesch10 = np.loadtxt('Pratika_data/oesch2018_uvlf_z10.txt')


# In[9]:


# z = 5
bouwens5_mag = bouwens5[:,0]
bouwens5_numd = bouwens5[:,1]
bouwens5_errl = abs(bouwens5_numd-bouwens5[:,3])
bouwens5_erru = abs(-bouwens5_numd+bouwens5[:,2])

fin5_mag = fin5[:,0]
fin5_numd = np.log10(fin5[:,1])
lerru = np.log10(fin5[:,5]+fin5[:,1])
lerrl = np.log10(fin5[:,1]-fin5[:,4])
fin5_errl = abs(fin5_numd - lerrl)
fin5_erru = abs(lerru - fin5_numd)

hari5_mag = hari5[:,0]
hari5_numd = np.log10(hari5[:,1])
lerru = np.log10(hari5[:,3]+hari5[:,1])
lerrl = np.log10(hari5[:,1]-hari5[:,2])
hari5_errl = abs(hari5_numd - lerrl)
```

```
hari5_erru = abs(lerru - hari5_numd)


# In[10]:


# z = 6
bouwens6_mag = bouwens6[:,0]
bouwens6_numd = np.log10(bouwens6[:,1])
lerru = np.log10(bouwens6[:,1]+bouwens6[:,2])
lerrl = np.log10(bouwens6[:,1]-bouwens6[:,2])
bouwens6_errl = abs(bouwens6_numd - lerrl)
bouwens6_erru = abs(lerru - bouwens6_numd)

fin6_mag = fink6[:,0]
fin6_numd = np.log10(fink6[:,1])
lerru = np.log10(fink6[:,3]+fink6[:,1])
lerrl = np.log10(fink6[:,1]-fink6[:,2])
fin6_errl = abs(fin6_numd - lerrl)
fin6_erru = abs(lerru - fin6_numd)

hari6_mag = hari6[:,0]
hari6_numd = np.log10(hari6[:,1])
lerru = np.log10(hari6[:,3]+hari6[:,1])
lerrl = np.log10(hari6[:,1]-hari6[:,2])
hari6_errl = abs(hari6_numd - lerrl)
hari6_erru = abs(lerru - hari6_numd)


# In[11]:


# z = 7
bouwens7_mag = bouwens7[:,0]
bouwens7_numd = np.log10(bouwens7[:,1])
lerru = np.log10(bouwens7[:,1]+bouwens7[:,2])
lerrl = np.log10(bouwens7[:,1]-bouwens7[:,2])
bouwens7_errl = abs(bouwens7_numd - lerrl)
bouwens7_erru = abs(lerru - bouwens7_numd)

Bowler7_mag = Bowler7[:,0]
Bowler7_numd = Bowler7[:,1]
Bowler7_errl = abs(Bowler7_numd-Bowler7[:,2])
Bowler7_erru = abs(-Bowler7_numd+Bowler7[:,3])

fin7_mag = fink7[:,0]
fin7_numd = np.log10(fink7[:,1])
lerru = np.log10(fink7[:,5]+fink7[:,1])
```

```
lerrl = np.log10(fink7[:,1]-fink7[:,4])
fin7_errl = abs(fin7_numd - lerrl)
fin7_erru = abs(lerru - fin7_numd)

hari7_mag = hari7[:,0]
hari7_numd = np.log10(hari7[:,1])
lerru = np.log10(hari7[:,3]+hari7[:,1])
lerrl = np.log10(hari7[:,1]-hari7[:,2])
hari7_errl = abs(hari7_numd - lerrl)
hari7_erru = abs(lerru - hari7_numd)


# In[12]:


# z = 8
ishi8_mag = ishi8[:,0]
ishi8_numd = ishi8[:,1]
ishi8_errl = abs(ishi8_numd-ishi8[:,2])
ishi8_erru = abs(-ishi8_numd+ishi8[:,3])

Bowler8_mag = Bowler8[:,0]
Bowler8_numd = np.log10(Bowler8[:,1])
lerru = np.log10(Bowler8[:,3]+Bowler8[:,1])
lerrl = np.log10(Bowler8[:,1]-Bowler8[:,2])
Bowler8_errl = abs(Bowler8_numd - lerrl)
Bowler8_erru = abs(lerru - Bowler8_numd)

fin8_mag = fink8[:,0]
fin8_numd = np.log10(fink8[:,1])
lerru = np.log10(fink8[:,5]+fink8[:,1])
lerrl = np.log10(fink8[:,1]-fink8[:,4])
fin8_errl = abs(fin8_numd - lerrl)
fin8_erru = abs(lerru - fin8_numd)

bouwens8_mag = bouwens8[:,0]
bouwens8_numd = np.log10(bouwens8[:,1])
lerru = np.log10(bouwens8[:,1]+bouwens8[:,2])
lerrl = np.log10(bouwens8[:,1]-bouwens8[:,2])
bouwens8_errl = abs(bouwens8_numd - lerrl)
bouwens8_erru = abs(lerru - bouwens8_numd)


# In[13]:


#  z= 9
ishi9_mag = ishi9[:,0]
```

```
ishi9_numd = ishi9[:,1]
ishi9_errl = abs(ishi9_numd-ishi9[:,2])
ishi9_erru = abs(-ishi9_numd+ishi9[:,3])

bouwens9_mag = Bouwens9[:,0]
bouwens9_numd = np.log10(Bouwens9[:,1])
lerru = np.log10(Bouwens9[:,1]+Bouwens9[:,2])
lerrl = np.log10(Bouwens9[:,1]-Bouwens9[:,2])
bouwens9_errl = abs(bouwens9_numd - lerrl)
bouwens9_erru = abs(lerru - bouwens9_numd)

Bowler9_mag = Bowler20_9[:,0]
Bowler9_numd = np.log10(Bowler20_9[:,1])
lerru = np.log10(Bowler20_9[:,3]+Bowler20_9[:,1])
lerrl = np.log10(Bowler20_9[:,1]-Bowler20_9[:,2])
Bowler9_errl = abs(Bowler9_numd - lerrl)
Bowler9_erru = abs(lerru - Bowler9_numd)

bouwenslbg9_mag = Bouwenslbg9[:,0]
bouwenslbg9_numd = np.log10(Bouwenslbg9[:,1])
lerru = np.log10(Bouwenslbg9[:,1]+Bouwenslbg9[:,2])
lerrl = np.log10(Bouwenslbg9[:,1]-Bouwenslbg9[:,2])
bouwenslbg9_errl = abs(bouwenslbg9_numd - lerrl)
bouwenslbg9_erru = abs(lerru - bouwenslbg9_numd)


# In[14]:


# z = 10
hari10_mag = hari10[:,0]
hari10_numd = np.log10(hari10[:,3])
lerru = np.log10(hari10[:,5]+hari10[:,3])
lerrl = np.log10(hari10[:,3]-hari10[:,4])
hari10_errl = abs(hari10_numd - lerrl)
hari10_erru = abs(lerru - hari10_numd)

bouwens10_mag = bouwens10[:,0]
bouwens10_numd = np.log10(bouwens10[:,1])
lerru = np.log10(bouwens10[:,1]+bouwens10[:,2])
lerrl = np.log10(bouwens10[:,1]-bouwens10[:,2])
bouwens10_errl = abs(bouwens10_numd - lerrl)
bouwens10_erru = abs(lerru - bouwens10_numd)

oesch10_mag = oesch10[:,0]
oesch10_numd = np.log10(oesch10[:,3])
lerru = np.log10(oesch10[:,2]+oesch10[:,3])
lerrl = np.log10(oesch10[:,3]-oesch10[:,2])
```

```
oesch10_errl = abs(oesch10_numd - lerrl)
oesch10_erru = abs(lerru - oesch10_numd)


# In[16]:


sfe_eye = [0.0008, 0.0012, 0.0017, 0.0022, 0.0025, 0.0015]

#plotting

fig, axs = plt.subplots(2,3,figsize=(15,7), sharex=True, sharey=True)
i = 1
axs[0,0].errorbar(hari5_mag, hari5_numd, yerr=[hari5_errl, hari5_erru], fmt='o',
axs[0,0].errorbar(bouwens5_mag, bouwens5_numd, yerr=[bouwens5_errl, bouwens5_erru
axs[0,0].errorbar(fin5_mag, fin5_numd, yerr=[fin5_errl, fin5_erru], fmt='o', labe
axs[0,0].set_ylabel('Number density ($cMPc^{-3}$)')

i = 2
axs[0,1].errorbar(hari6_mag, hari6_numd, yerr=[hari6_errl, hari6_erru], fmt='o',
axs[0,1].errorbar(fin6_mag, fin6_numd, yerr=[fin6_errl, fin6_erru], fmt='o', labe
axs[0,1].errorbar(bouwens6_mag, bouwens6_numd, yerr=[bouwens6_errl,bouwens6_erru]


i=3
axs[0,2].errorbar(hari7_mag, hari7_numd, yerr=[hari7_errl, hari7_erru], fmt='o',
axs[0,2].errorbar(fin7_mag, fin7_numd, yerr=[fin7_errl, fin7_erru], fmt='o', labe
axs[0,2].errorbar(bouwens7_mag, bouwens7_numd, yerr=[bouwens7_errl, bouwens7_erru
axs[0,2].errorbar(Bowler7_mag, Bowler7_numd, yerr = [Bowler7_errl, Bowler7_erru],


i=4
axs[1,0].errorbar(ishi8_mag, ishi8_numd, yerr=[ishi8_errl, ishi8_erru], fmt='o',
axs[1,0].errorbar(fin8_mag, fin8_numd, yerr=[fin8_errl, fin8_erru], fmt='o', labe
axs[1,0].errorbar(bouwens8_mag, bouwens8_numd, yerr= [bouwens8_errl, bouwens8_err
axs[1,0].errorbar(Bowler8_mag, Bowler8_numd, yerr = [Bowler8_errl, Bowler8_erru],
axs[1,0].set_ylabel('Number density ($cMPc^{-3}$)')
axs[1,0].set_xlabel('Magnitude')

i=5
axs[1,1].errorbar(ishi9_mag, ishi9_numd, yerr=[ishi9_errl, ishi9_erru], fmt='o',
axs[1,1].errorbar(bouwens9_mag, bouwens9_numd, yerr= [bouwens9_errl, bouwens9_err
axs[1,1].errorbar(bouwenslbg9_mag, bouwenslbg9_numd, yerr=[bouwenslbg9_errl, bouw
axs[1,1].errorbar(Bowler9_mag, Bowler9_numd, yerr = [Bowler9_errl, Bowler9_erru],
axs[1,1].set_xlabel('Magnitude')

i=6
axs[1,2].errorbar(hari10_mag, hari10_numd, yerr=[hari10_errl, hari10_erru], fmt=
```

```
axs[1,2].errorbar(bouwens10_mag, bouwens10_numd, yerr=[bouwens10_errl, bouwens10_
axs[1,2].errorbar(oesch10_mag, oesch10_numd, yerr=[oesch10_errl, oesch10_erru], f
axs[1,2].set_xlabel('Magnitude')
i=0
for j in range(2):
    for k in range(3):
        if i < 6:
            axs[j,k].plot(magsim[i+1], numd[i+1], color=CB_color_cycle[3], label=
            axs[j,k].plot(mag(SFGf(mass[i],sfe_eye[i])), numd[i], color=CB_color_
            i = i+1
            axs[j,k].set_ylim(-10,2)
            axs[j,k].invert_xaxis()
            axs[j,k].legend()
i = 1
for ax in axs.flat:
    ax.set(ylim=[-10.5,1.9], xlim= [-13, -29])
    ax.text(-15,-9, 'z={}'.format(i+4), fontsize=20)
    ax.tick_params(axis='y', direction='in')
    ax.tick_params(axis='x', direction='in')
    ax.legend()
    i  = i+1
fig.tight_layout(w_pad=0, h_pad=0)
plt.show()


# In[18]:


Z = np.linspace(5,10,6)
z = np.linspace(4, 10, 7)

product_fit = 0.048*np.array(sfe_eye)
plt.scatter(z, sfe(z), color=CB_color_cycle[3], label='Pacucci ')
plt.scatter(Z, np.log10(sfe_eye), color=CB_color_cycle[-1], label='Abundance mat
plt.legend()
plt.ylabel('log(f)')
plt.xlabel('z')
plt.show()


# In[ ]:


omdm = 0.262
omb = 0.048
fs = np.linspace(0, 0.2,100)
gs = np.linspace(0, omb/omdm, 100)
```

```
F, G = np.meshgrid(fs, gs)

# z=5
f5 =  interp1d(numd[1], mass[1])
numd5 = [*bouwens5_numd, *fin5_numd, *hari5_numd]
mag5 = np.array([*bouwens5_mag, *fin5_mag, *hari5_mag])
exp = f5(numd5)
obs = mag5

x5 = np.zeros((100,100))

for i in range(len(fs)):
    for j in range(len(gs)):
        X5, P5 = chisquare(obs, f_exp=mag(SFGf(exp, fs[i], gs[j])))
        x5[i,j] = X5

# z=6
f6 =  interp1d(numd[2], mass[2])
numd6 = [*bouwens6_numd, *fin6_numd, *hari6_numd]
mag6 = np.array([*bouwens6_mag, *fin6_mag, *hari6_mag])
exp = f6(numd6)
obs = mag6

x6 = np.zeros((100,100))

for i in range(len(fs)):
    for j in range(len(gs)):
        X6, P = chisquare(obs, f_exp=mag(SFGf(exp, fs[i], gs[j])))
        x6[i,j] = X6

# z=7
f7 =  interp1d(numd[3], mass[3])
numd7 = [*bouwens7_numd, *fin7_numd, *hari7_numd, *Bowler7_numd]
mag7 = np.array([*bouwens7_mag, *fin7_mag, *hari7_mag, *Bowler7_mag])
exp = f7(numd7)
obs = mag7

x7 = np.zeros((100,100))

for i in range(len(fs)):
    for j in range(len(gs)):
        X, P = chisquare(obs, f_exp=mag(SFGf(exp, fs[i], gs[j])))
        x7[i,j] = X

# z=8
f8 =  interp1d(numd[4], mass[4])
numd8 = [*bouwens8_numd, *fin8_numd, *ishi8_numd, *Bowler8_numd]
mag8 = np.array([*bouwens8_mag, *fin8_mag, *ishi8_mag, *Bowler8_mag])
```

```
exp = f8(numd8)
obs = mag8

x8 = np.zeros((100,100))

for i in range(len(fs)):
    for j in range(len(gs)):
        X, P = chisquare(obs, f_exp=mag(SFGf(exp, fs[i], gs[j])))
        x8[i,j] = X

# z=9
f9 =  interp1d(numd[5], mass[5])
numd9 = [*bouwens9_numd, *bouwenslbg9_numd, *ishi9_numd, *Bowler9_numd]
mag9 = np.array([*bouwens9_mag, *bouwenslbg9_mag, *ishi9_mag, *Bowler9_mag])
exp = f9(numd9)
obs = mag9

x9 = np.zeros((100,100))

for i in range(len(fs)):
    for j in range(len(gs)):
        X, P = chisquare(obs, f_exp=mag(SFGf(exp, fs[i], gs[j])))
        x9[i,j] = X

# z=10
f10 =  interp1d(numd[6], mass[6])
numd10 = [*bouwens10_numd, *hari10_numd, *oesch10_numd]
mag10 = np.array([*bouwens10_mag, *hari10_mag, *oesch10_mag])
exp = f10(numd10)
obs = mag10

x10 = np.zeros((100,100))

for i in range(len(fs)):
    for j in range(len(gs)):
        X, P = chisquare(obs, f_exp=mag(SFGf(exp, fs[i], gs[j])))
        x10[i,j] = X


# In[ ]:


x = np.linspace(0.001, 0.19, 1000)
low_estimate = [8e-5, 1e-4, 2e-4, 2e-4, 2e-4, 2e-4]
hig_estimate = [3.5e-4, 5.5e-4, 6e-4, 1e-3, 1.3e-3, 1.2e-3]

normalizer=Normalize(-60,0)
im=cm.ScalarMappable(norm=normalizer)
```

```
fig , axs = plt.subplots(2,3,figsize=(15,7))

i=0
im5 = axs[0,0].imshow(x5, origin='lower', extent = [0,omb/omdm, 0, 0.2], norm=nor
axs[0,0].axvline()
axs[0,0].set_ylim(0, 0.2)
axs[0,0].set_xlim(0, omb/omdm)
axs[0,0].set_xlabel('baryonic␣matter␣fraction')
axs[0,0].set_ylabel('$f$')

i=1
im6 = axs[0,1].imshow(x6, origin='lower', extent = [0,omb/omdm, 0, 0.2], norm=nor
axs[0,1].set_ylim(0, 0.2)
axs[0,1].set_xlim(0, omb/omdm)
axs[0,1].set_xlabel('baryonic␣matter␣fraction')
axs[0,1].set_ylabel('$f$')

i=2
im7 = axs[0,2].imshow(x7, origin='lower', extent = [0,omb/omdm, 0, 0.2], norm=nor
axs[0,2].set_ylim(0, 0.2)
axs[0,2].set_xlim(0, omb/omdm)
axs[0,2].set_xlabel('baryonic␣matter␣fraction')
axs[0,2].set_ylabel('$f$')

i=3
im8 = axs[1,0].imshow(x8, origin='lower', extent = [0,omb/omdm, 0, 0.2], norm=nor
axs[1,0].set_ylim(0, 0.2)
axs[1,0].set_xlim(0, omb/omdm)
axs[1,0].set_xlabel('baryonic␣matter␣fraction')
axs[1,0].set_ylabel('$f$')

i=4
im9 = axs[1,1].imshow(x9, origin='lower', extent = [0,omb/omdm, 0, 0.2], norm=nor
axs[1,1].set_ylim(0, 0.2)
axs[1,1].set_xlim(0, omb/omdm)
axs[1,1].set_xlabel('baryonic␣matter␣fraction')
axs[1,1].set_ylabel('$f$')

i=5
im10 = axs[1,2].imshow(x10, origin='lower', extent = [0,omb/omdm, 0, 0.2], norm=n
axs[1,2].set_ylim(0, 0.2)
axs[1,2].set_xlim(0, omb/omdm)
axs[1,2].set_xlabel('baryonic␣matter␣fraction')
axs[1,2].set_ylabel('$f$')

i=0
for j in range(2):
```

```
    for k in range(3):
        axs[j,k].plot(x, low_estimate[i]/x, color='black')
        axs[j,k].plot(x, hig_estimate[i]/x, color='black')
        i = i+1
i = 1
for ax in axs.flat:
    ax.text(0.13,0.15, 'z={}'.format(i+4), fontsize=20)
    ax.tick_params(axis='y')
    ax.tick_params(axis='x' )
    i  = i+1

fig.tight_layout()
cax,kw = mpl.colorbar.make_axes([ax for ax in axs.flat])
cb = plt.colorbar(im, cax=cax, **kw)
cb.set_label('$\chi^2$ test statistic')
plt.show()


# In[ ]:


def SFGf(m, f):
    '''Halo mass to luminosity for a star forming galaxy using fitted f, just the
    m = 10**m * M_sun
    L1500 = 10**33.07*u.erg/u.s/M_sun/u.Angstrom
    return (f*m*L1500).cgs

fig, axs = plt.subplots(2,3,figsize=(15,7), sharex=True, sharey=True)

i = 1
# axs[0,0].plot(mag(SFGf(mass[i],SFE[i])), numd[i], color=CB_color_cycle[-1], lab
axs[0,0].errorbar(hari5_mag, hari5_numd, yerr=[hari5_errl, hari5_erru], fmt='o',
axs[0,0].errorbar(bouwens5_mag, bouwens5_numd, yerr=[bouwens5_errl, bouwens5_erru
axs[0,0].errorbar(fin5_mag, fin5_numd, yerr=[fin5_errl, fin5_erru], fmt='o', labe
axs[0,0].plot(mag(SFGf(mass[i], low_estimate[i-1])), numd[i], color= CB_color_cy
axs[0,0].plot(mag(SFGf(mass[i], hig_estimate[i-1])), numd[i], color= CB_color_cy
axs[0,0].set_ylabel('Number density ($cMPc^{-3}$)')

i = 2
# axs[0,1].plot(mag(SFGf(mass[i],SFE[i])), numd[i], color=CB_color_cycle[-1], lab
axs[0,1].errorbar(hari6_mag, hari6_numd, yerr=[hari6_errl, hari6_erru], fmt='o',
axs[0,1].errorbar(fin6_mag, fin6_numd, yerr=[fin6_errl, fin6_erru], fmt='o', labe
axs[0,1].errorbar(bouwens6_mag, bouwens6_numd, yerr=[bouwens6_errl,bouwens6_erru]
axs[0,1].plot(mag(SFGf(mass[i], low_estimate[i-1])), numd[i], color= CB_color_cy
axs[0,1].plot(mag(SFGf(mass[i], hig_estimate[i-1])), numd[i], color= CB_color_cy

i=3
# axs[0,2].plot(mag(SFGf(mass[i],SFE[i])), numd[i], color=CB_color_cycle[-1], lab
```

```
axs[0,2].errorbar(hari7_mag, hari7_numd, yerr=[hari7_errl, hari7_erru], fmt='o',
axs[0,2].errorbar(fin7_mag, fin7_numd, yerr=[fin7_errl, fin7_erru], fmt='o', labe
axs[0,2].errorbar(bouwens7_mag, bouwens7_numd, yerr=[bouwens7_errl, bouwens7_erru
axs[0,2].errorbar(Bowler7_mag, Bowler7_numd, yerr = [Bowler7_errl, Bowler7_erru],
axs[0,2].plot(mag(SFGf(mass[i], low_estimate[i-1])), numd[i], color= CB_color_cy
axs[0,2].plot(mag(SFGf(mass[i], hig_estimate[i-1])), numd[i], color= CB_color_cy

i=4
# axs[1,0].plot(mag(SFGf(mass[i],SFE[i])), numd[i], color=CB_color_cycle[-1], lab
axs[1,0].errorbar(ishi8_mag, ishi8_numd, yerr=[ishi8_errl, ishi8_erru], fmt='o',
axs[1,0].errorbar(fin8_mag, fin8_numd, yerr=[fin8_errl, fin8_erru], fmt='o', labe
axs[1,0].errorbar(bouwens8_mag, bouwens8_numd, yerr= [bouwens8_errl, bouwens8_err
axs[1,0].errorbar(Bowler8_mag, Bowler8_numd, yerr = [Bowler8_errl, Bowler8_erru],
axs[1,0].plot(mag(SFGf(mass[i], low_estimate[i-1])), numd[i], color= CB_color_cy
axs[1,0].plot(mag(SFGf(mass[i], hig_estimate[i-1])), numd[i], color= CB_color_cy
axs[1,0].set_xlabel('Magnitude')
axs[1,0].set_ylabel('Number density ($cMPc^{-3}$)')

i=5
# axs[1,1].plot(mag(SFGf(mass[i],SFE[i])), numd[i], color=CB_color_cycle[-1], lab
axs[1,1].errorbar(ishi9_mag, ishi9_numd, yerr=[ishi9_errl, ishi9_erru], fmt='o',
axs[1,1].errorbar(bouwens9_mag, bouwens9_numd, yerr= [bouwens9_errl, bouwens9_err
axs[1,1].errorbar(bouwenslbg9_mag, bouwenslbg9_numd, yerr=[bouwenslbg9_errl, bouw
axs[1,1].errorbar(Bowler9_mag, Bowler9_numd, yerr = [Bowler9_errl, Bowler9_erru],
axs[1,1].plot(mag(SFGf(mass[i], low_estimate[i-1])), numd[i], color= CB_color_cy
axs[1,1].plot(mag(SFGf(mass[i], hig_estimate[i-1])), numd[i], color= CB_color_cy
axs[1,1].set_xlabel('Magnitude')

i=6
# axs[1,2].plot(mag(SFGf(mass[i],SFE[i])), numd[i], color=CB_color_cycle[-1], lab
axs[1,2].errorbar(hari10_mag, hari10_numd, yerr=[hari10_errl, hari10_erru], fmt='
axs[1,2].errorbar(bouwens10_mag, bouwens10_numd, yerr=[bouwens10_errl, bouwens10_
axs[1,2].errorbar(oesch10_mag, oesch10_numd, yerr=[oesch10_errl, oesch10_erru], f
axs[1,2].plot(mag(SFGf(mass[i], low_estimate[i-1])), numd[i], color= CB_color_cy
axs[1,2].plot(mag(SFGf(mass[i], hig_estimate[i-1])), numd[i], color= CB_color_cy
axs[1,2].set_xlabel('Magnitude')

i = 1
for ax in axs.flat:
    ax.set(ylim=[-10.5,1.9], xlim= [-13, -29])
    ax.text(-15,-9, 'z={}'.format(i+4), fontsize=20)
    ax.tick_params(axis='y', direction='in')
    ax.tick_params(axis='x', direction='in')
    ax.legend()
    i  = i+1
fig.tight_layout(w_pad=0, h_pad=0)
plt.show()
```

```
# In[ ]:


fig, ax = plt.subplots(2,3,figsize=(15,7), sharex=True, sharey=True)
i=0
for j in range(2):
    for k in range(3):
        x = np.linspace(rmin[i], rmax[i], 100)
        ax[j,k].fill_between(x, low_estimate[i]/x, hig_estimate[i]/x, color= CB_
        i = i+1
        if j == 1:
            ax[j,k].set_xlabel('Baryonic matter fraction')
        if k == 0:
            ax[j,k].set_ylabel('f')
i=1
for axs in ax.flat:
    axs.text(0.15,0.014, 'z={}'.format(i+4), fontsize=20)
    axs.tick_params(axis='y', direction='in')
    axs.tick_params(axis='x', direction='in')
    i  = i+1
fig.tight_layout(w_pad=0, h_pad=0)
plt.show()
```